Journal of Solid State Chemistry 182 (2009) 65–71

Contents lists available at ScienceDirect

Journal of Solid State Chemistry

journal homepage: www.elsevier.com/locate/jssc

$(NH_4)[V^{III}_{1-x}V^{IV}_x(AsO_4)F_{1-x}O_x]$: A new mixed valence vanadium(III,IV) fluoro-arsenate with ferromagnetic interactions and electronic conductivity

Teresa Berrocal [a], José L. Mesa [b,*], José L. Pizarro [a], Begoña Bazán [a], Idoia Ruiz de Larramendi [b], María I. Arriortua [a], Teófilo Rojo [b]

[a] Departamento de Mineralogía y Petrología, Facultad de Ciencia y Tecnología, Universidad del País Vasco/EHU, Apdo. 644, E-48080 Bilbao, Spain
[b] Departamento de Química Inorgánica, Facultad de Ciencia y Tecnología, Universidad del País Vasco/EHU, Apdo. 644, E-48080 Bilbao, Spain

ARTICLE INFO

Article history:
Received 1 July 2008
Received in revised form
18 September 2008
Accepted 2 October 2008
Available online 14 October 2008

Keywords:
Hydrothermal synthesis
Mixed valent V(III, IV) arsenate
Crystal structure
ESR
Ferromagnetism
Electronic conductivity

ABSTRACT

A new mixed valence vanadium(III,IV) fluoro-arsenate compound, with formula $(NH_4)[V^{III}_{1-x}V^{IV}_x(AsO_4)F_{1-x}O_x]$ and KTP structure-type, has been synthesized by mild hydrothermal techniques. The crystal structure has been solved from single crystal X-ray diffraction data in the $Pna2_1$ orthorhombic space group. The unit-cell parameters are $a = 13.196(2)$ Å, $b = 6.628(1)$ Å and $c = 10.7379(7)$ Å with $Z = 8$. The final R factors were $R1 = 0.0438$ and w$R2 = 0.0943$ [all data]. The crystal structure consists of a three-dimensional framework formed by $(V^{III,IV}O_4F_2)$ octahedra and $(AsO_4)^{3-}$ tetrahedra arsenate oxoanions. The vanadium(III,IV) cations, from the $(V^{III,IV}O_4F_2)$ octahedra, are linked through the fluorine atoms giving rise to zigzag chains. The ammonium cations are located in the cavities of the structure compensating the anionic charge of the $[V^{III}_{1-x}V^{IV}_x(AsO_4)F_{1-x}O_x]^-$ inorganic skeleton. The thermal stability limit of the phase is 345 °C, around to this temperature the ammonium cation and fluoride anion are lost. The IR spectrum shows the characteristic bands of the $(NH_4)^+$ and $(AsO_4)^{3-}$ ions. Magnetic measurements indicate the existence of weak ferromagnetic interactions. Electronic conductivity, via a hopping mechanism, occurs with an activation energy of 0.66 eV.

1. Introduction

The research on phosphate, phosphite and arsenate materials with new open framework structures is currently in progress due to their potential application in catalysis, gas separation, ion exchange, biological systems and electromagnetic and optical functions [1–3]. The synthetic technique used to obtain this type of compounds is hydrothermal synthesis. This method has been successful in the preparation of important solids such as KTP compounds, microporous crystals [4], superionic conductors [5], complex oxides ceramics and fluorides [6,7] and magnetic materials [8–10]. Addition of fluoride anions into the reaction mixture, developed by Ferey et al. [11–13], has led to the discovery of the new microporous structural types, some of them exhibiting very large channels such as in cloverite [14]. In these phases, the fluoride anions participate in the coordination sphere of the metal ion. A systematic study of the fluorine systems [11,12] has shown that the geometry of the structure's directing agent plays an important role in the attainment of three-dimensional open frameworks. It has also been observed that the ammonium groups from the organic molecules preferentially interact with the fluorine atoms of the framework via hydrogen bonds.

A particular kind of opened frameworks can be obtained by hydrothermal synthesis and these phases exhibit a characteristic structure type KTP ($KTiOPO_4$) [15]. This structure's family of compounds presents very interesting characteristics due to its electro-optical properties and of nonlinear optical (NLO) [16]. The structure of $KTiOPO_4$ was first determined by Tordjman et al. [15]. KTP crystallizes in the noncentrosymmetric orthorhombic space group $Pna2_1$, with lattice parameters $a = 12.814(6)$ Å, $b = 6.404(2)$ Å and $c = 10.616(5)$ Å. The structure is characterized by helical chains of (TiO_6) octahedra that are linked at two corners and are separated by (PO_4) tetrahedra. Alternating long and short Ti–O bonds occur along these chains that result in a net z-directed polarization and are the major contributors to the large nonlinear optic an electro-optic coefficients. There are 10 equivalent oxygen sites per unit cell. The potassium ion is located in a high coordination number site and is bonded to the oxygen atoms in the (TiO_6) octahedra and (PO_4) tetrahedra. Channels exist along the [0 0 1] and [0 1 0] direction, whereby potassium ions can diffuse via a vacancy mechanism [17]. The cation diffusion through these channels influences the ionic conductivity and ferroelectricity properties. Research has centred on developing the technology related to the conditions of the synthesis, in order to

* Corresponding author. Fax: +00 34 946013500.
E-mail address: joseluis.mesa@ehu.es (J.L. Mesa).

0022-4596/$ - see front matter © 2008 Elsevier Inc. All rights reserved.
doi:10.1016/j.jssc.2008.10.002

reproduce new phases with high quality KTP structure, with a potential high place in the non linear optics and in the construction of optical and electro-optical devices. The family of compounds, KTP, is very extensive today. The general formula is $MM'OXO_4$ where M = K, Rb, Na, Cs, Tl, NH_4; M' = Ti, Sn, Sb, Zr, Ge, To, Cr, V, Nb, Ta; X = P, As. The nature of M, M' and X has direct consequences on the properties of these compounds [18]. In this sense, some partially substituted KTP material, such as $KTi(AsO_4)$, $RbTiO(AsO_4)$ and $RbTi_{0.98}Zr_{0.02}O(PO_4)$, exhibit conductivity [19].

In this work we present on a new KTP-type phase, $(NH_4)[V^{III}_{1-x}V^{IV}_x(AsO_4)F_{1-x}O_x]$, which is isoestructural to the $(NH_4)[V(PO_4)F]$ compound [20]. Here, we report on the hydrothermal synthesis, crystal structure, thermal behavior, conductivity and magnetic properties of this mixed valent vanadium(III,IV) fluoroarsenate KTP-compound. The title compound is the second example in the $(NH_4)[V(XO_4)F]$ (X = P and As) family of phases that exhibits ferromagnetic exchange couplings.

2. Experimental section

2.1. Synthesis and chemical analysis

$(NH_4)[V^{III}_{1-x}V^{IV}_x(AsO_4)F_{1-x}O_x]$ has been synthesized by using mild hydrothermal conditions under autogeneous pressure. The reagents VCl_3, $As_2O_5.nH_2O$ and HF, in a molar ratio of 0.026:0.127:1, were solved in distilled water (30 mL), and then ammonium hydroxide was added to adjust the pH of the solution to approximately 4.5. This solution was sealed in a PTFE-lined steel pressure vessel for 5 days at 170 °C, after which the resulting product was slowly cooled to room temperature. Black single-crystals were obtained, filtered and washed with water and acetone, and finally, dried in air. The yield was approximately 80%. The density was measured by the flotation method using a mixture of iodometane (CH_2I_2, $\rho = 3.325\,g\,cm^{-3}$) and chloroform (Cl_3CH, $\rho = 1.492\,g\,cm^{-3}$), obtaining an experimental density of $\rho_{exp} = 3.14(1)\,g\,cm^{-3}$.

Vanadium and arsenic contents were calculated by ICP-EAS spectroscopy. The nitrogen and hydrogen contents were measured by elemental analysis. The amount of the fluoride anions was calculated by using a selective electrode. The values obtained from the analysis are: V: 22.4(1); As: 33.0(1); N: 6.2(1); H: 1.8(1); F: 7.8(1) %.

2.2. Single-crystal X-ray diffraction

A black single-crystal with the dimensions $0.11 \times 0.11 \times 0.13$ mm was carefully selected under a polarizing microscope and mounted on a glass fiber. Single-crystal X-ray diffraction data were collected at room temperature on an Oxford Diffraction XCALIBUR2 automated diffractometer (Mo$K\alpha$ radiation) equipped with a SAPPHIRE 2-CCD detector. Of the 7137 reflections measured, 2408 were unique with a R_{int} factor of 0.0579. The number of observed reflections with $I > 2\sigma(I)$ was 2025. The diffractometer software [21] was used to carry out the Lorentz-polarization and absorption corrections, taking into account the size and the shape of the crystal, as well as the data reduction procedure. The structure was solved by direct methods using the SHELXS97 program [22] in the $Pna2_1$ space group. The SHELXL 97 program [23] was used to refine the structure by the least-square method based on F^2. Scattering factors were taken from Ref. [24]. All the atoms belonging to the framework were initially located except fluorine, and nitrogen atoms, which were definitively assigned while refining the structure. The H atoms of the ammonium cation could not be located.

On the other hand, the value of 0.47(2) obtained for the Flack parameter in the refinement of the structure was a clear indication for the racemic twinning in the crystal studied. Consequently, the final refinement was performed including a correction for twinning by inversion, obtaining values of $R1 = 0.0384$ [$I > 2\sigma(I)$] and BASF = 0.513. All atoms were anisotropically refined. The final R-factors were $R1 = 0.0438$ and $wR2 = 0.0943$ for all data. The structure drawings were performed using the ATOMS program [25]. The structure factor parameters have been deposited at the Cambridge Crystallographic Data Centre (CCDC 419640).

The bond valence analysis of the refined structural model, was carried out with the Brown and Altermatt method [26], using the $s = \exp[(r_0 - r)/B]$ expression in which r_0 are 1.743 and 1.702 Å for the V–O and V–F bond distances, $B = 0.37$ Å in both kind of bonds and r the experimental V–O, F values of the bond lengths, with results of V(1) 3.28 and V(2) 3.16 v.u. These values are higher than those expected for the existence of only V(III) cations in the composition of this phase (see Table 1).

Table 1 shows a charge of less than −2 on the oxygen atoms, which can be compensated for by the contribution of the hydrogen atoms when the possible hydrogen bonds are established. The excess of charge on the V(III) cations suggests a change in the oxidation state of the metallic cations from V(III) to V(IV). Although structural refinements were carried out taking into account the partial substitution of fluoride anions by oxygen atoms, the results were unsuccessful. So, the final proposed formula of this phase, $(NH_4)[V^{III}_{1-x}V^{IV}_x(AsO_4)F_{1-x}O_x]$, was established taking into account the simultaneous existence of V(III) and V(IV) cations in the composition, in a proportion that could not be determined by X-ray diffraction.

2.3. Physicochemical characterization techniques

The IR spectrum (KBr pellets) was obtained with a Nicolet FT-IR 740 spectrophotometer in the spectral range of 400–4000 cm^{-1}. A Bruker ESP 300 spectrometer, operating at X band, was used to record the ESR polycrystalline spectrum at 300 K. Magnetic measurements on the powdered sample were performed in the temperature range 4.5–300 K at 1000 Gauss, using a Quantum Design MPMS-7 SQUID magnetometer. The applied magnetic field was 0.1 T, a value in the range of linear dependence of magnetization vs. magnetic field, even at 4.5 K. For the electrical

Table 1
Bond valance analysis in $(NH_4)[V^{III}_{1-x}V^{IV}_x(AsO_4)F_{1-x}O_x]$

	O (1)	O (2)	O (3)	O (4)	O (5)	O (6)	O (7)	O (8)	F (1)	F (2)	Σ
V (1)			0.435	0.468	0.586			0.497	0.744	0.556	3.287
V (2)	0.569	0.499				0.477	0.557		0.389	0.669	3.161
As (1)	1.190		1.242				1.235	1.269			4.937
As (2)		1.249		1.312	1.233	1.232					5.027
Amount	1.759	1.748	1.677	1.78	1.819	1.709	1.792	1.766	1.133	1.225	

property measurements a pellet from the sample (4.96 mm diameter and 0.88 mm thickness) was used and coated with platinum meshes as an electrode. Electrochemical impedance spectroscopy (EIS) measurements were conducted using a Solartron 1260 impedance analyzer. The frequency range was 10^{-2}–10^{6} Hz with a signal amplitude of 300 mV. All of these electrochemical experiments were performed at equilibrium from 340 °C to room temperature, under zero dc current intensity and under air over a cycle of heating and cooling. Impedance diagrams were analyzed and fitted by the equivalent circuit method using Zview software. Resistance and capacitance values from the fitting of each semicircle in the EIS measurements were obtained by least square refinement.

3. Results and discussion

3.1. Description of the structure

Crystallographic data, atomic coordinates and selected bond distances and angles are listed in Tables 2–4, respectively.

The structure of $(NH_4)[V^{III}_{1-x}V^{IV}_{x}(AsO_4)F_{1-x}O_x]$ is described as a three-dimensional framework constructed from corner-sharing (VO_4F_2) octahedra and (AsO_4) tetrahedra. Chains formed by alternating (V(1)O_4F_2) or (V(2)O_4F_2) octahedra and (As(1)O_4) or (As(2)O_4) tetrahedra, respectively, are running along the [1 0 0] and [0 1 0] directions, and are linked by a common oxygen vertex (Fig. 1). The chains are interconnected through the fluorine atoms belonging to the (VO_4F_2) octahedra. This architecture forms six-ring channels along the *a*- and *b*-axis in which the ammonium cations are located in two different crystallographic positions (see Supplementary material). The $(NH_4)^+$ groups compensate for the anionic charge of the $[V(AsO_4)F]^-$ inorganic skeleton, establishing hydrogen bonds with both the fluorine and oxygen atoms. This structural framework is similar to that found in the KTiO(PO_4)-type materials.

In both octahedra, the vanadium(III,IV) cations are linked to the oxygen atoms belonging to the (AsO_4) tetrahedra with a mean V–O bond distance of 1.98(5) Å. The hexacoordination is completed with two fluoride ions bonded at a mean bond distance of 1.961(9) Å. The cis- and trans-O,F–V–O,F bond angles ranges are between 81.0(2)–99.2(2) and 168.2(1)–177.6(3), respectively, as expected for slightly distorted octahedral geometry around the vanadium(III) cations. The distortion of the (V(1)O_4F_2) and (V(2)O_4F_2) octahedra and (As(1)O_4) and (As(2)O_4) tetrahedra from that of an ideal octahedron and tetrahedron, evaluated by the Alvarez et al. method [27], is $S(Oh) = 0.313$, 0.08 and $S(Td) = 0.133$, 0.052, respectively, for each polyhedron. The arsenic atoms are in tetrahedral coordination with an average As–O bond distance of 1.68(1) Å, and O–As–O angles near 109(2)°, as expected in the arsenate compounds with sp^3 hybridization.

The hydrogen contacts established between the ammonium cations and the fluorine and oxygen atoms of the $[V(AsO_4)F]^-$ network are in the 2.703(9)–3.430(9) and 2.840(8)–3.360(9) Å range, for N…O and N…F, respectively.

Table 2
Crystallographic data and structure refinement parameters for $(NH_4)[V^{III}_{1-x}V^{IV}_{x}(AsO_4)F_{1-x}O_x]$

Formula	$(NH_4)[V^{III}_{1-x}V^{IV}_{x}(AsO_4)F_{1-x}O_x]$
Molecular weight (g mol^{-1})	226.90
Crystal system	Orthorhombic
Space group (No. 33)	$Pna2_1$
a (Å)	13.196(2)
b (Å)	6.628(1)
c (Å)	10.738(1)
v (Å^3)	939.1(2)
Z	8
ρ_{obs}, ρ_{calc} (g cm^{-3})	3.14(1), 3.21
F(0 0 0)	864
Temperature (K)	293(2)
Diffractometer	Oxford diffraction *X*calibur2
μ (mm^{-1})	9.050
Radiation, λ(Mo*K*α) (Å)	0.71073
Limiting indices h k l	$-18 \leqslant h \leqslant 18$, $K \pm 9$, $-13 \leqslant h \leqslant 15$
R (int)	0.0579
R [I > 2σ(I)]	*R*1 = 0.0390, w*R*2 = 0.0928
R (all data)	*R*1 = 0.0438, w*R*2 = 0.0943
G.O.F.	1.003

$R1 = [(|F_o| - |F_c|)]/|F_o|$; $wR2 = [[w(|F_o|^2 - |F_c|^2)^2]/[w(|F_o|^2)^2]]^{1/2}$. $w = 1/[\sigma^2|F_o|^2 + (xp)^2 + yp]$, where $p = [|F_o|^2 + 2|F_c|^2]/3$; $x = 0.0447$; $y = 0.0$.

Table 3
Atomic coordinates and equivalent thermal parameters ($U_{eq} \times 10^3$) for $(NH_4)[V^{III}_{1-x}V^{IV}_{x}(AsO_4)F_{1-x}O_x]$

ATOM	*x*	*y*	*z*	U(eq)
As (1)	0.1819 (1)	0.5040 (1)	0.9590 (1)	7 (1)
As (2)	−0.0008 (1)	0.1757 (1)	0.7065 (1)	7 (1)
V (1)	0.1227 (1)	0.0014 (1)	0.9540 (2)	11 (1)
V (2)	0.2477 (1)	0.2626 (1)	0.7023 (2)	12 (1)
O (1)	0.2373 (4)	0.0461 (9)	0.5798 (5)	13 (1)
O (2)	0.1003 (2)	0.3279 (5)	0.6873 (6)	11 (1)
O (3)	0.1095 (3)	0.3024 (6)	0.9950 (4)	9 (1)
O (4)	−0.0151 (4)	0.0160 (8)	0.5879 (5)	14 (1)
O (5)	0.0124 (4)	0.0335 (10)	0.8361 (5)	13 (1)
O (6)	−0.1061 (2)	0.3167 (5)	0.7272 (5)	12 (1)
O (7)	0.2609 (4)	0.4572 (10)	0.8387 (5)	14 (1)
O (8)	0.1072 (3)	−0.2965 (6)	0.9297 (5)	15 (1)
F (1)	0.2183 (4)	0.0509 (8)	0.8369 (8)	22 (1)
F (2)	0.2202 (4)	−0.0457 (8)	1.0833 (5)	21 (1)
N (1)	0.1059 (4)	−0.3108 (8)	0.5262 (6)	29 (1)
N (2)	−0.1091 (5)	0.7183 (9)	0.7792 (7)	35 (1)

$U_{eq} = 1/3[U_{11}(aa^*)^2 + U_{22}(bb^*)^2 + U_{33}(cc^*)^2 + 2U_{13}aca^*c^*\cos\beta]$.

3.2. Thermal behavior

The thermogravimetric analysis (TGA) was performed under synthetic air in a DSC 2960 simultaneous DSC-TGA instrument. A crucible containing ca. 20 mg of sample was heated at 5 °C min^{-1} in the 30–500 °C temperature range. The TG curve shows a mass loss of 1%, between room temperature and 100 °C, probably due to the loss of the adsorbed water. This process continues with the loss of another 25% of mass, from 100 to 420 °C. This loss corresponds to a superposition between different processes. The first one, the loss of 16%, from approximately 100–385 °C, corresponds to the elimination of both the ammonium cations and fluoride anions, and the second one corresponds to the decomposition of the vanadium (III,IV) arsenate, between 385 and 420 °C, and supposes an experimental mass loss of 9%. The sharp peak observed at 400 °C in the DTA curve indicates that both the calcination of the ammonium cations and the elimination of the fluoride anions are exothermic processes. Above 420 °C, the TG curve continues decreasing due to the decomposition of the arsenate groups and the formation of the inorganic residues, which spread into the crucible. This fact precluded its characterization.

Thermal behavior was also studied by using time-resolved X-ray thermodiffractometry in air. A PHILIPS X′PERT diffractometer (Cu*K*α radiation) equipped with a variable-temperature stage (Paar Physica) with a Pt sample heater, was used (Fig. 2). The powder patterns were recorded in 2θ steps of 0.02° in the range $10 \leqslant 2\theta \leqslant 38°$, counting for 2 s per step and recording the diagrams

Table 4
Selected bond distances (Å) and angles (°) for (NH_4) $[V^{III}_{1-x}V^{IV}_{x}(AsO_4)F_{1-x}O_x]$

V (1)	O (3)	O (4)^{iii}	O (5)	O (8)	F (1)	F (2)
F (2)	93.4 (2)	87.0 (2)	173.4 (2)	90.1 (2)	93.68 (14)	1.919 (5)
F (1)	91.8 (2)	172.8 (3)	92.9 (2)	99.2 (3)	1.811 (5)	
O (8)	168.19 (16)	88.0 (2)	87.0 (2)	2.001 (4)		
O (5)	88.3 (2)	86.78 (14)	1.941 (5)			
O (4)^{iii}	81.0 (2)	2.024 (6)				
O (3)	2.051 (4)					
V (2)	O (1)	O (2)	O (6)^{v}	O (7)	F (1)	F (2)^{iv}
F (2)^{iv}	93.2 (3)	91.0 (2)	93.0 (2)	92.53 (19)	177.6 (3)	1.851 (5)
F (1)	87.63 (17)	91.2 (2)	84.8 (2)	86.6 (3)	2.051 (5)	
O (7)	173.8 (4)	90.2 (2)	89.3 (2)	1.959 (5)		
O (6)^{v}	88.0 (2)	176.0 (3)	2.017 (4)			
O (2)	92.1 (2)	2.000 (4)				
O (1)	1.951 (5)					
[As (1)O_4] tetrahedron						
As (1)	O (1)ii	O (3)	O (7)	O (8)^{i}		
O (8)^{i}	112.4 (3)	109.52 (15)	111.4 (3)	1.679 (4)		
O (7)	103.06 (15)	112.3 (2)	1.689 (5)			
O (3)	108.1 (3)	1.687 (4)				
O (1)^{ii}	1.703 (5)					
[As (2)O_4] tetrahedron						
As (2)	O(2)	O(4)	O(5)	O(6)		
O (6)	109.54 (14)	111.0 (3)	106.5 (3)	1.690 (3)		
O (5)	110.7 (3)	106.65 (19)	1.690 (6)			
O (4)	112.1 (3)	1.666 (5)				
O (2)	1.685 (3)					

Symmetry codes: i = $x, y+1, z$; ii = $-x+1/2, y+1/2, z+1/2$; iii = $-x, -y, z+1/2$; iv = $-x+1/2, y+1/2, z-1/2$; v = $x+1/2, -y+1/2, z$; vi = $-x+1/2, y-1/2, z-1/2$; vii = $-x, -y, z-1/2$; viii = $x-1/2, -y+1/2, z$; ix = $x, y-1, z$; x = $-x+1/2, y-1/2, z+1/2$.

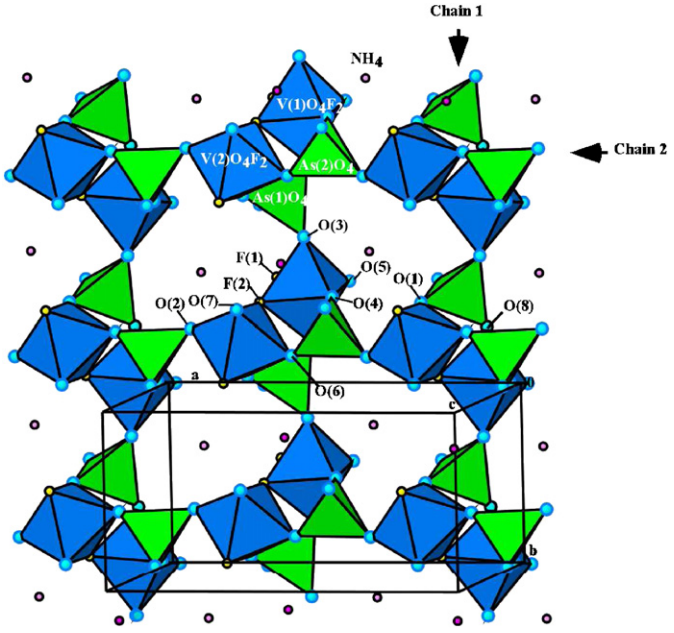

Fig. 1. Polyhedral view of the [100] and [010] chains in the $(NH_4)[V^{III}_{1-x}V^{IV}_{x}(AsO_4)F_{1-x}O_x]$ compound.

every 15 °C min^{-1} from room temperature up to 700 °C. The diffractograms indicate that thermal stability limit is 345 °C, which is the temperature at which the structure collapses, due to the calcination of the ammonium cations and the elimination of the fluoride anions. In the 345–390 °C range no peaks were observed in the diffractograms, which indicates that the collapse of the crystal structure gives rise to an amorphous product. Between 390 and 630 °C, the appearance of vanadium oxides and arsenates can be observed. At the highest temperature of 700 °C, the $(VO)(AsO_4)$ (tetragonal, $a = b = 6.33$, $c = 4.18$ Å) [28a], (V_2O_5) (tetragonal, $a = b = 14.259$, $c = 12.57$ Å [28b], (V_2O) (monoclinic, $a = 20.54$, $b = 20.43$, $c = 25.05$ Å, $\beta = 90.5(^\circ)$] [28c] and (VO_2) (triclinic, $a = 9.06$, $b = 5.77$, $c = 4.52$ Å, $\alpha = 89.99$, $\beta = 91.40$, $\gamma = 89.83^\circ$) [28d] phases are detected in the inorganic residue.

3.3. IR spectroscopy

The infrared spectrum shows the characteristic bands of the ammonium cations and $(AsO_4)^{3-}$ arsenate oxoanions. The stretching mode of the $(NH_4)^+$ group appears in the 2700–3100 cm^{-1} range. The bands near 1420 cm^{-1} can be assigned to the bending vibration of this cation. Three different groups of bands can be attributed to the vibrational modes of $(AsO_4)^{3-}$. The asymmetric, ν_{as}(As–O), stretching mode appears at 860, 830 and 805 cm^{-1}. The symmetric, ν_s(As–O), stretching vibration is detected at 680 cm^{-1}. Finally, the asymmetrical deformation vibration, δ_{as}(O–As–O), appears at 500 and 480 cm^{-1}. The positions of the vibrational bands of both the ammonium cation and arsenate oxoanion are similar to those reported in the literature [29].

3.4. Magnetic properties

3.4.1. ESR measurements

The ESR spectrum of $(NH_4)[V^{III}_{1-x}V^{IV}_{x}(AsO_4)F_{1-x}O_x]$ shows a weak signal corresponding to the V(IV)-d^1 cations at approximately

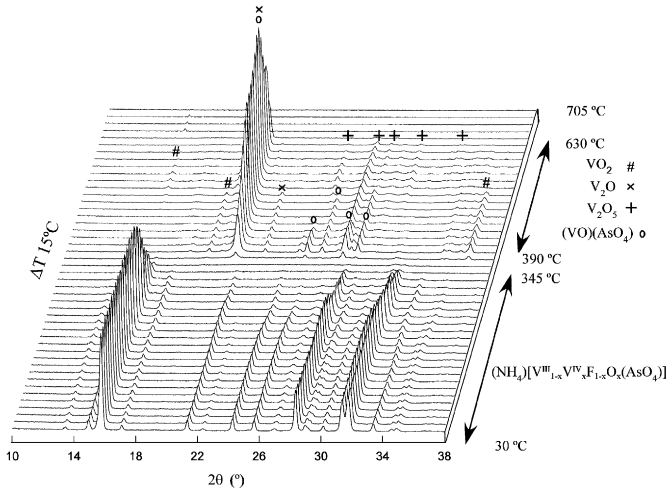

Fig. 2. Thermodiffractograms of $(NH_4)[V^{III}_{1-x}V^{IV}_{x}(AsO_4)F_{1-x}O_x]$.

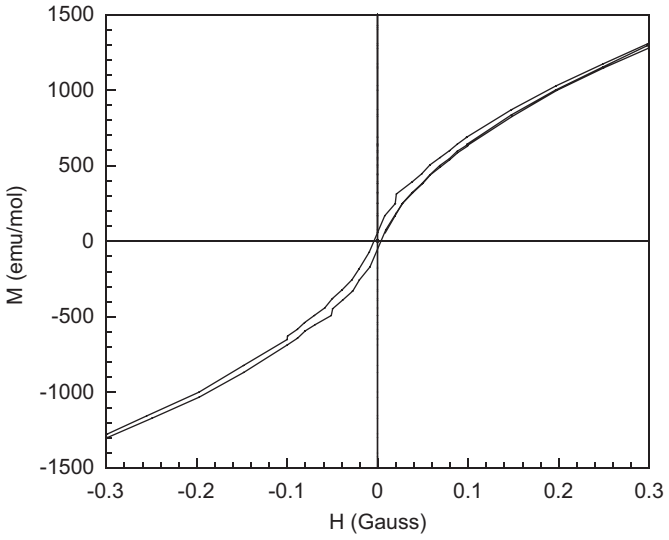

Fig. 4. Hysteresis loop at 2.0 K of $(NH_4)[V^{III}_{1-x}V^{IV}_{x}(AsO_4)F_{1-x}O_x]$.

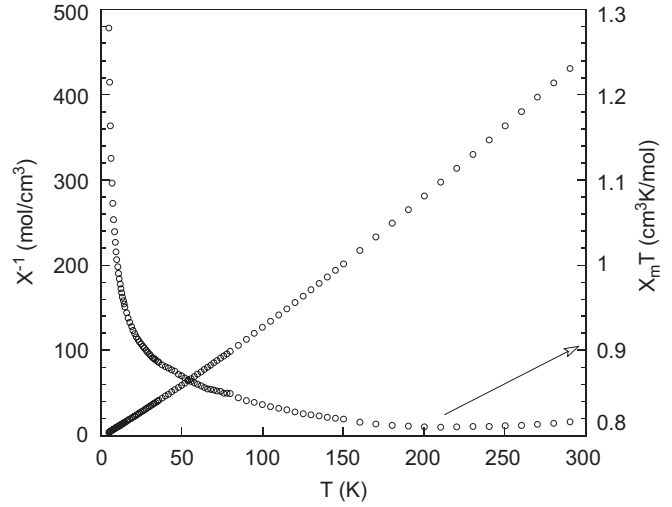

Fig. 3. Thermal variation of χ_m^{-1} and $\chi_m T$ curves for $(NH_4)[V^{III}_{1-x}V^{IV}_{x}(AsO_4)F_{1-x}O_x]$.

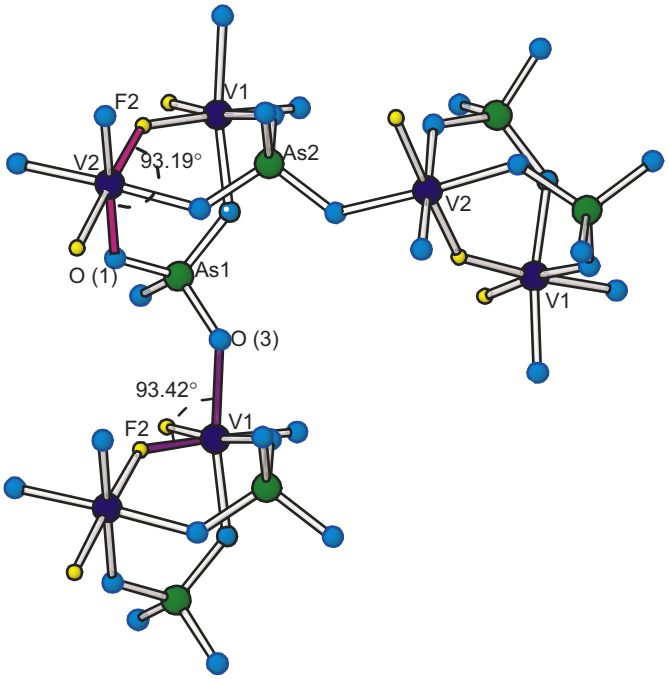

Fig. 5. Magnetic exchange pathways for $(NH_4)[V^{III}_{1-x}V^{IV}_{x}(AsO_4)F_{1-x}O_x]$.

3200 Gauss. The enhancement of the signal above zero in the intensity axis (see Supplementary material) is probably caused by the zero field splitting parameter of the V(III)-d^2 cations [30], that exist together with the V(IV) ions in this phase and indicate the mixed valence nature of this phase.

3.4.2. *Magnetization measurements*

The thermal evolution of the χ_m^{-1} and $\chi_m T$ curves is shown in Fig. 3. The measured data were fitted to a Curie–Weiss law $[\chi_m = C_m/(T-\theta)]$ with $C_m = 0.682\ cm^3\ K\ mol^{-1}$ and $\theta = 7.3$ K. The $\chi_m T$ vs. T curve increases continuously from $0.815\ cm^3\ K\ mol^{-1}$ at room temperature, up to $1.277\ cm^3\ K\ mol^{-1}$at 4.5 K. This result and the positive Weiss temperature indicate the existence of weak ferromagnetic exchange interactions. The evolution of the imanation vs. magnetic field shows a small hysteresis loop, with values of the coercive field and remnant magnetization of 0.01 Gauss and 75 emu mol^{-1}, respectively (see Fig. 4), corroborating the existence of weak ferromagnetic couplings in this phase.

Considering the three-dimensional framework of the title compound two intermetallic exchange pathways can be distinguished between the V(III,IV) cations (see Fig. 5). The mean value of the O–V–F bond angles is 93.8(1)°. This value is near the orthogonal angle and supports the ferromagnetic behavior observed in this phase [31].

A comparison between the $(NH_4)[V(XO_4)F]$ (X = P and As) and $(NH_4)[Fe(PO_4)F]$ [32] isomorphous compounds shows the same three-dimensional framework with corner-sharing octahedra, in which the metallic cations are linked through fluoride ions with M–F–M angles of approximately 130° in the phosphate phases [18,32], and approximately 139° in the arsenate compound. However the magnetic behavior of these compounds is different. In this way, the iron(III) phosphate shows antiferromagnetic exchange interactions with a Weiss temperature of approximately −230 K and an ordering temperature near to 75 K, whereas the two $(NH_4)[V(XO_4)F]$ (X = P and As) vanadium phases are ferromagnetically coupled with a small Weiss temperature,

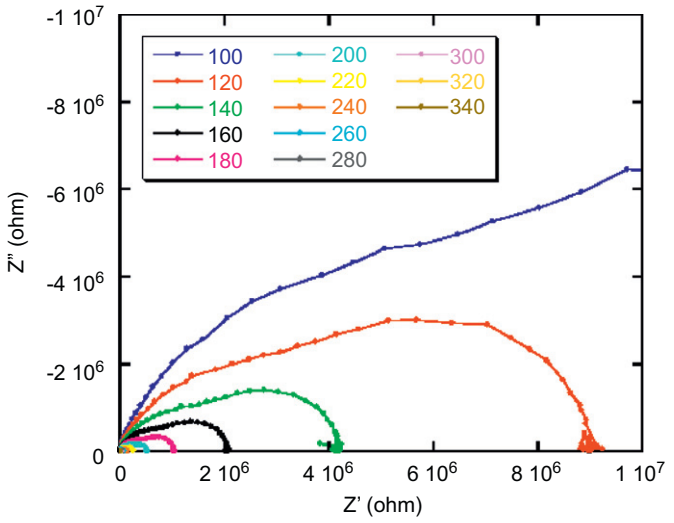

Fig. 6. Thermal evolution of the Nyquist's diagrams $(NH_4)[V^{III}_{1-x}V^{IV}_{x}(AsO_4)F_{1-x}O_x]$.

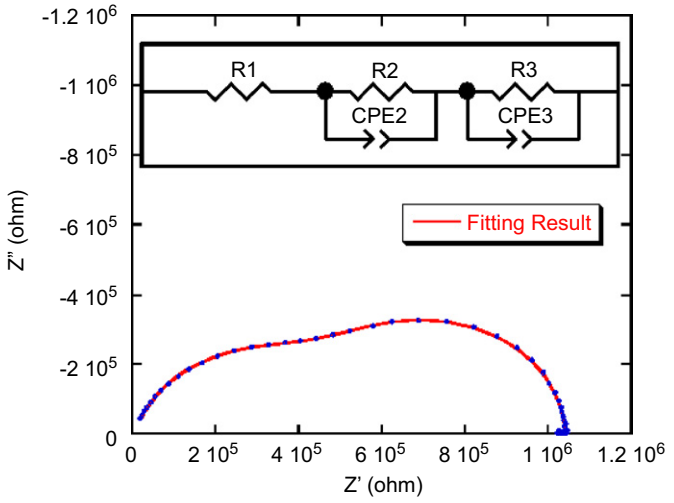

Fig. 7. Fit of the Nyquist's diagrams at 180 °C for $(NH_4)[V^{III}_{1-x}V^{IV}_{x}(AsO_4)F_{1-x}O_x]$. The inset shows the equivalent circuit used for the fitting.

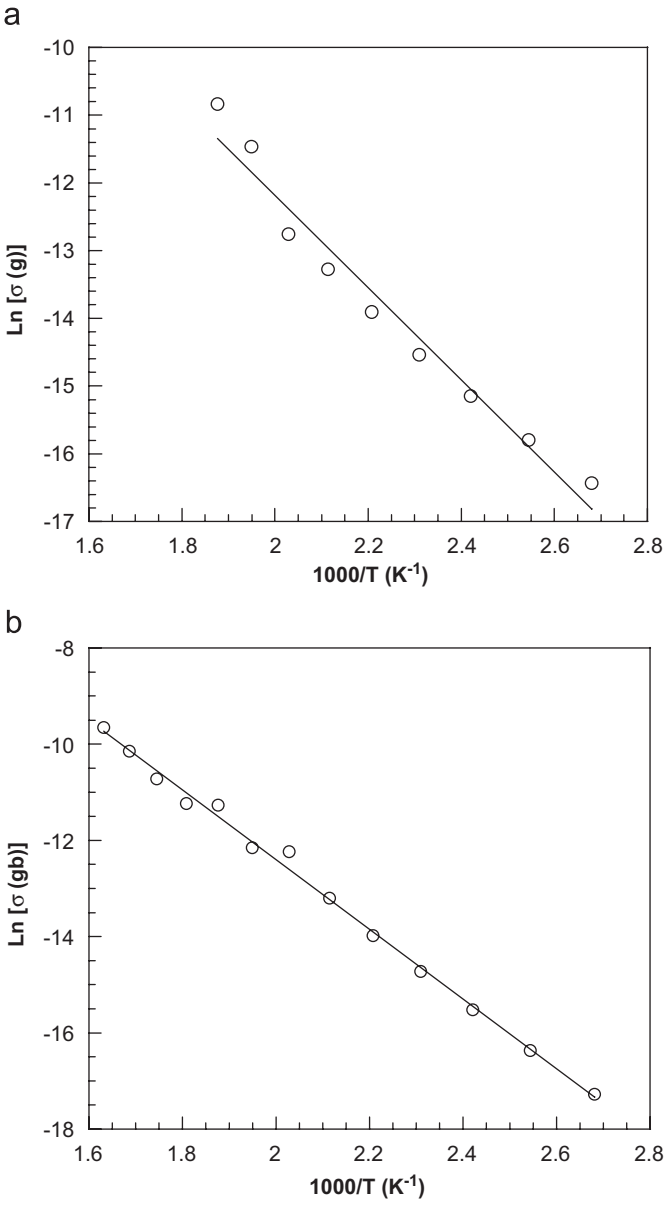

Fig. 8. Arrhenius's plots of the (a) $\sigma(g)$ and (b) $\sigma(gb)$ for $(NH_4)[V^{III}_{1-x}V^{IV}_{x}(AsO_4)F_{1-x}O_x]$.

$\theta = 2.7$ ($X = P$) and 7.3 K ($X = As$). This difference in sign of the magnetic interactions observed in the Fe(III) vs. V(III) and V(III,IV) phases could be associated with the reduction in the number of possible magnetic exchange pathways that take place in the vanadium(III)-d^2 cation and vanadium(IV)-d^1 cation in comparison with the d^5 high spin iron(IIII) compound.

3.5. Impedance spectroscopy

The real (Z') and imaginary part (Z'') of the impedance measurements are shown in Fig. 6, where an overlapping of two semicircles is observed. The experimental data were fitted using an equivalent circuit consisting of three resistances ($R_{1,2,3}$) and two constant phase elements in parallel (CPE2 and CPE3). Fig. 7 shows the fit of the spectrum recorded at 180 °C to this equivalent circuit.

From the fit of the spectra, the resistance and CPE values at different temperatures were obtained. The first data were used to calculate de conductivity values, and the second enabled us to calculate the capacitance values of each process (Supplementary material). Fig. 8 shows the Arrhenius plots for the thermal evolution of the grain conductivity [$\sigma(g)$] and grain boundary conductivity [$\sigma(gb)$], which have the energy activations of 0.56 and 0.59 eV, respectively. These values are in the typical range of those observed for semiconductor materials [33].

Taking into account the crystal structure of $(NH_4)[V^{III}_{1-x}V^{IV}_{x}(AsO_4)F_{1-x}O_x]$, in which the ammonium cations establish strong bonds with the inorganic framework, through ionic interactions and hydrogen bonds, it is possible to assign the observed conductivity to a electronic process, probably of a hopping type. This phenomenon is possible due to the simultaneous existence in this compound of vanadium cations in two different oxidation states, +III and +IV, in good agreement with the results obtained from the crystal structure refinement. Finally, the maximum value obtained for the electronic conductivity in this material, 6.44×10^{-5} S/cm, allows us to conclude that $(NH_4)[V^{III}_{1-x}V^{IV}_{x}(AsO_4)F_{1-x}O_x]$ presents a small conductivity level.

4. Concluding remarks

A new three-dimensional arsenate with formula $(NH_4)[V^{III}_{1-x}V^{IV}_{x}(AsO_4)F_{1-x}O_x]$ has been synthesized by using mild hydrothermal techniques under autogeneous pressure. The crystal structure of this compound is constructed by two perpendicular chains running along the [1 0 0] and [0 1 0] directions. These chains delimit six-ring channels in which the ammonium cations are located. The thermal behavior shows the elimination of ammonium cations and fluoride anions at approximately 345 °C. This process is followed by the collapse of the crystal structure. The IR spectroscopy confirms the presence of the arsenate anion and ammonium cation. Magnetic measurements indicate the presence of weak ferromagnetic couplings. The maximum value obtained for the electronic conductivity in this material is 6.44×10^{-5} S/cm.

Acknowledgments

This work has been financially supported by the "Ministerio de Educación y Ciencia" (MAT2007-60400/66737-C02-01) and the "Gobierno Vasco, Grupos de Investigación del Sistema Universitario Vasco (IT-177–07 and IT-312–07)". The authors would like to thank SGIker for technical support (MEC, GV/ES, European Social Fund). T. Berrocal wishes to thank the "Departamento de Investigación y Ciencia del Gobierno Vasco/Eusko Jaurlaritza" for funding.

References

[1] A.K. Cheetman, G. Ferey, T. Loiseau, Angew. Chem. Int. Ed. 38 (1999) 3268; J.-S. Chang, J.-S. Hwang, S.-H. Jung, S.-E. Park, G. Ferey, A.K. Cheetham, Angew. Chem. Int. Ed. 43 (2004) 2819.
[2] G.D. Stucky, M.L.F. Phillips, T.E. Gier, Chem. Mater. 1 (1999) 3268.
[3] M. Eddaoudi, D.B. Moler, H. Li, B. Chen, T. Reinekete, M. O'Keefe, O.M. Yaghi, Acc. Chem. Res. 34 (2001) 319.
[4] M. Estermann, L.B. McCusker, C. Baerlocher, A. Merrouche, H. Kessler, Nature 352 (1991) 320.
[5] Q.W. Chen, Y.T. Qian, Z.Y. Chen, K.B. Tang, G.E. Zhou, Y.H. Zhang, Physica C 224 (1994) 228.
[6] C. Zhao, S. Feng, R. Xu, C. Shi, J. Ni, Chem. Commun. (1997) 945.
[7] G. Ferey, T. Loiseau, D. Riou, Adv. Inorg. Fluor. 209 (2000).
[8] B. Bazan, J.L. Mesa, J.L. Pizarro, L. Lezama, A. Peña, M.I. Arriortua, T. Rojo, J. Solid State Chem. 17 (2006) 1459.
[9] B. Bazan, J.L. Mesa, J.L. Pizarro, L. Lezama, A. Peña, M.I. Arriortua, T. Rojo, Z. Anorg, Allg. Chem. 63 (2005) 2026.
[10] B. Bazan, J.L. Mesa, J.L. Pizarro, J. Rodríguez-Fernandez, J. Sanchez-Marcos, E. Molins, M.I. Arriortua, T. Rojo, Chem. Mater. 16 (2004) 5249.
[11] G. Ferey, J. Fluor. Chem. 72 (1995) 187.
[12] T. Loiseau, G. Ferey, J. Fluor. Chem. 128 (2007) 422–431.
[13] G. Ferey, T. Loiseau, D. Riou, In Advanced Inorganic Fluorides: Synthesis, Characterization and Applications, Elsevier, Science, New York, 2000.
[14] T. Loiseau, D. Riou, M. Licteron, G. Ferey, J. Solid State Chem. 111 (1994) 397.
[15] P.I. Tordjman, R. Masse, J.C. Guitel, Z. Kristallogr. 139 (1974) 103.
[16] G.D. Stucky, M.L.F. Phillyps, T.E. Gier, Chem. Mater. 1 (1989) 492–509.
[17] J. Bierlein, H.J. Vanherzeele, Opt. Soc. Am. B 6 (1989) 662.
[18] M. E Hagerman, K.R. Poeppelmeier, Chem Mater. 7 (1995) 602.
[19] J. Zhang, J. Wang, B. Ge, Y. Liu, X. Hu, G. Zhao, S. Zhu, R.I. Boughton, Opt. Mater. 28 (2006) 335; A.A. Alekseeva, A.P. Dudka, N.E. Novokova, N.I. Sorokina, E.I. Agapova, V.I. Voronkova, Crystallogr. Rep. 53 (2008) 557.
[20] E. Alda, B. Bazán, J.L. Mesa, J.L. Pizarro, M.I. Arriortua, T. Rojo, J. Solid State Chem. 173 (2003) 101.
[21] CRYSALIS, version 1.170.32, Oxford Diffraction Ltd., Oxford, 2003.
[22] G.M. Sheldrick, SHELXS97, Program for the Solution of Crystal Structures, University of Göttingen, Göttingen, Germany, 1997.
[23] G.M. Sheldrick, SHELXL97, Program for the Refinement of Crystal Structures, University of Göttingen, Göttingen, Germany, 1997.
[24] International Tables for X-ray Crystallography, vol. IV, Kynoch Press, Birmingham, England, p. 99.
[25] E. Dowty, ATOMS, A Computer Program for Displaying Atomic Structures, Shape Sotware, 521 Hidden Valley Road, Kingsport, TN, 1993.
[26] I.D. Brown, The Chemical Bond in Inorganic Chemistry, Oxford Science Publications, Oxford, 2002.
[27] S. Alvarez, D. Avnir, M. Lunell, M. Pinsky, New. J. Chem. 26 (2002) 996.
[28] Powder Diffraction File—Inorganic and Organic, Files No. 033-1446. Powder Diffraction File—Inorganic and Organic, Files No. 0-45-1074. Powder Diffraction File—Inorganic and Organic, Files No. 035-0361. Powder Diffraction File–Inorganic and Organic, Files No. 01-071-0288.
[29] K. Nakamoto, Infrared and Raman Spectra of Inorganic and Coordination Compounds, Wiley, New York, 1997.
[30] A. Bencini, D. Gatteschi, EPR of Exchange Coupled Systems, Springer, Berlin, Heidelberg, 1990.
[31] J.B. Goodenough, Magnetism and the Chemical Bond, Interscience, New York, 1963.
[32] Th. Loiseau, Y. Calage, P. Lacorre, G. Ferey, J. Solid State Chem. 111 (1994) 390.
[33] S. Ezhilvalavan, J.M. Xue, J. Wang, J. Phys. D: Appl. Phys 35 (2002) 2254; M.C. Ungureanu, M. Levy, J.L. Bouquet, Ceram. Silikaty 44 (3) (2000) 81.